Journal of
Synchrotron Radiation

ISSN 0909-0495

Received 16 June 2008
Accepted 16 September 2008

Diffraction of partially coherent X-rays in clessidra prism arrays

Liberato De Caro,[a] Werner Jark,[b]* Ralf Hendrik Menk[b] and Marco Matteucci[b]

[a]Istituto di Cristallografia – Consiglio Nazionale delle Ricerche (IC-CNR), via Amendola 122/O, I-70125 Bari, Italy, and [b]Sincrotrone Trieste ScpA, SS 14 km 163.5, I-34012 Basovizza (TS), Italy. E-mail: werner.jark@elettra.trieste.it

When small triangular prisms are arranged in arrays which have an overall appearance like an hourglass (in Italian: clessidra) they can focus X-rays owing to a combined action of diffraction and refraction. From the optical point of view these objects can be regarded as a Fresnel variant of concave transmission lenses. Consequently they can provide larger apertures than purely refractive lenses. However, one has to recognize that clessidra lenses will strongly diffract as the lens structure is periodic in the direction perpendicular to the incident beam. In experiments the diffraction is reduced because it is difficult to illuminate the large apertures with a full spatially coherent wavefront. So the illumination is at best partially coherent. In order to interpret available experimental data for this condition, diffraction theory has been applied appropriately to the clessidra structure, taking into account the limited spatial coherence. The agreement between the theoretical simulations and experimental data is very good, keeping the lens properties at their projected values and allowing for only two free model parameters. The first is the lateral spatial coherence; the second is a lens defect, a rounding of all edges and tips in the structure. Both values obtained from the simulations have been found to be in agreement with expectations.

Keywords: X-ray optics; kinoform lens; refraction; diffraction; spatial coherence.

1. Introduction

Clessidra prism array lenses fall into the category of X-ray transmission lenses. This category is presently studied extensively after the first practical X-ray transmission lenses were introduced in 1996 by Snigirev *et al.* (1996). A systematic comparison of the properties of lenses of different concepts in this field is presented by Jark *et al.* (2006). The construction concept for the simplest clessidra lens is shown in Fig. 1. For the purpose of this paper we should note that the structure is a kinoform lens (Lesem *et al.*, 1969). In fact it is obtained from a purely refractive lens of concave shape (Lengeler *et al.*, 1999) by removing blocks of optically passive material (Jark *et al.*, 2004). These latter blocks are dimensioned for shifting the phase of the transmitted wavefronts compared with the adjacent structures such that wavefront contiguity is maintained in the transmitted longitudinally periodic wavefield. This strategy was first proposed for the focusing of X-rays by Suehiro *et al.* (1991).

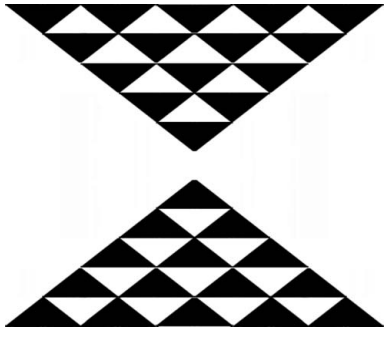

Figure 1
Construction principle of the clessidra lens composed of identical triangular prisms.

In most of the technical realisations the absorption was minimized, leading to decreasing segment heights with increasing distance from the optical axis (Aristov *et al.*, 2000; Nöhammer *et al.*, 2003; Evans-Lutterodt *et al.*, 2003, 2007; Nazmov *et al.*, 2004). In clessidra lenses (Jark *et al.*, 2004) the absorption losses grow linearly with distance from the optical axis. The same holds true for the prism array of slightly different shape presented by Cederström *et al.* (2005). Any kinoform concept will provide larger apertures than purely refractive lenses of concave shape with the same focal length (Jark *et al.*, 2006). This provides a twofold advantage for the focusing of X-rays; firstly it will allow for the collection of more photon flux, and secondly it will permit a smaller diffraction-limited focus size. The drawbacks are that kinoform lenses function optimally only at single wavelengths and

that present state-of-the-art lithographic production techniques can only produce one-dimensionally focusing objects (Aristov *et al.*, 2000; Nöhammer *et al.*, 2003; Evans-Lutterodt *et al.*, 2003, 2007; Nazmov *et al.*, 2004; Pérennès *et al.*, 2005; Cederström *et al.*, 2005).

An advantageous feature of the simple clessidra structure is the relatively simple control of the shape fidelity even in optical microscopes. However, we have to recognize that the clessidra lenses, as well as the Cederström prism arrays, are highly periodically structured perpendicularly to the incident beam. So these lenses are diffracting the incident radiation like linear transmission gratings. The diffractive focal length of such objects for the photon wavelength λ is (Jark *et al.*, 2006)

$$f_{\rm diff} = h^2/m\lambda, \tag{1}$$

where m is a multiple of 2π phase shifts in the transmitted radiation along any prism base compared with travel in air, and h is the prism height perpendicular to the incident beam.

The immediately obvious question for this simplified structure in Fig. 1 is then: can it really concentrate most of the incident photon flux into a single line, and can the related line width s be smaller than h, once the demagnified source image is expected to be smaller than h? A theoretical study by De Caro & Jark (2008) answered this question affirmatively with very promising perspectives for the present lens concept. As long as the incident wave can be assumed to be a spatially coherent plane wave over the whole aperture of the lens in the focusing direction, the photon flux distribution in the focal plane of a prism array can be derived from an analytical expression. The solution can be expressed even for generalized unitless distance parameters and is thus rather universally applicable. As long as the distortion introduced by the straight prisms into the transmitted wavefield remains below the Rayleigh quarterwave criterion (Born & Wolf, 1980), more than 80% of the transmitted photon flux is diffracted into the principal diffraction peak. This is the case for $|m| \leq 2$. The missing photon flux is diffracted into well separated secondary diffraction peaks, which can be suppressed by appropriately positioned apertures between the lens and the focus. Under these conditions the full width at half-maximum (FWHM) of the principal peak of the photon flux distribution coincides with the diffraction-limited spot size obtainable with the chosen lens aperture. The line width is thus completely independent of the shape and the dimensions of the single prisms. Interestingly the secondary diffraction peaks can even be eliminated by curving some prism side walls appropriately.

As far as obtainable line width is concerned, a clessidra would be competitive for X-ray microfocusing if it could provide a focal length of the order of 0.1 m for wavelengths below λ = 0.154 nm. From Jark *et al.* (2006) we would then expect a state-of-the-art diffraction-limited line width of the order of 50 nm (Schroer *et al.*, 2005) for a relatively large geometric aperture of A = 0.4 mm. However, according to (1) this requires prism heights of the order of h = 4 µm. In order to predict whether straight prisms can be realised by use of lithography with this size and without systematic defects, that might dominate the transmission losses, we produced prototype lenses with larger prism heights of the order of 20 µm, in which the shape fidelity could be guaranteed to a large amount. The final lenses have apertures in the millimeter range, which is much larger than the spatially coherently illuminated areas at reasonable source distances even from particularly small synchrotron radiation sources. In this case we deal with only partially coherent illumination and the focus size is thus source size limited. In fact, all the reported tests for kinoform lenses were made under these conditions (Aristov *et al.*, 2000; Nöhammer *et al.*, 2003; Evans-Lutterodt *et al.*, 2003, 2007; Nazmov *et al.*, 2004; Jark *et al.*, 2006; Cederström *et al.*, 2005). So in order to be able to derive the lens imperfections from the focusing defects, we need to include the limited spatial coherence in the theoretical treatment. This problem will be treated rigorously in the theoretical part of this study. More commonly used approximations and simplifications will not allow us to maintain the correlation between the nature of a lens defect and an observed focus defect. In order to better model real lenses, we also added for this purpose an eventually possible rounding of the prism tips and shallow angles (edges), the only identifiable defect visible in light microscopes. The experimental part will then compare the expectations with the measured data.

2. Theoretical part

2.1. Phase shift introduced by a clessidra lens made of real prisms

As in our previous study (De Caro & Jark, 2008), we will treat the diffraction of partially coherent X-ray wavefields by one-dimensionally focusing clessidra lenses as a one-dimensional problem. The beam travels in the y direction and is focused in the x direction; $x = 0$ refers to the optical axis of the experimental set-up. Moreover, we assume to be in a thin lens situation, where the overall object extension in the beam direction (longitudinal lens size $L_{\rm size}$) is significantly smaller than its focal length f. In fact, as long as $L_{\rm size}/f$ is much less than 10^{-1}, one can use a local approximation for the modification of the incident wavefield caused by the lens, assuming the lens to be simply a planar object (Snigirev *et al.*, 1998; Kohn *et al.*, 2003).

Introducing the unitless off-axis distance $\bar{x} = x/h$, where h is the prism height in the jth row of a clessidra lens constructed of perfect prisms, we can write the lens propagator $P(j, \bar{x})$ as follows (De Caro & Jark, 2008),

$$\begin{aligned} P(j,\bar{x}) &= \exp\left(-i\pi m\bar{x}^2\right)\exp\left[i\pi m(\bar{x}-j)^2\right]\exp\left[i\pi m\left(j^2-|j|\right)\right] \\ &\quad\times\exp[i2\pi m\bar{w}(x,j)] \\ &= P_{\rm id}(j,\bar{x})\exp[i2\pi m\bar{w}(x,j)]. \end{aligned} \tag{2}$$

Here, the dimensionless parameter $m = b\delta/\lambda$ is defined as $m = m_0 + \Delta m - im_0\beta/\delta$, where b is the prism base length. At the correct operation energy one would find the 'ideal' value $b_{\rm id}$ such that m_0 is an integer value, *i.e.* the number of 2π phase-shifts in any prism. Δm is introduced in order to allow for an incorrect photon energy setting. The imaginary part is related to the absorption. The four phase terms of (2) are due,

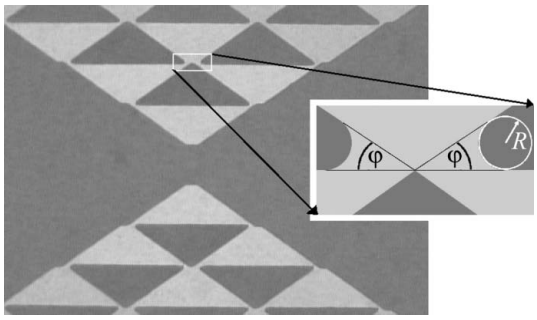

Figure 2
Micrograph from the center part of a clessidra lens of the type in Fig. 1 with parameters identical to those studied in this report. Prism height and width are $h = 25.67$ μm and $b = 73.3$ μm, respectively. The white rectangle indicates a position where the rounding was modeled according to the details in the inset. Inset: schematic drawing of the spherical meniscus with radius of curvature R formed at the intersection between tips and bases of prisms belonging to different rows. φ is the angle between the lateral sides and bases of prisms belonging to different rows.

respectively, to (i) the ideal parabolic profile; (ii) the correction between the clessidra with straight side walls and the parabolic profile; (iii) the missing blocks of optically inactive material; (iv) the material distribution $\bar{w}(j, \bar{x}) = w(j, \bar{x})/b_{\rm id}$ caused by the presence of a spherical meniscus of curvature radius R, between the tips of prisms of the $(j-1)$th row and the bases of prisms of the jth row, as shown in the inset of Fig. 2. The first three contributions define the propagator of an ideal clessidra lens $P_{\rm id}(j, \bar{x})$. The last phase contribution is due to the finite size and shape of real tips. For $R \rightarrow 0$ one has $P \rightarrow P_{\rm id}$.

The amount of extra material owing to the spherical menisci shown in the inset in Fig. 2 is calculated under the condition of a tangent circle of radius R on the prism side walls. Thus, putting $\bar{R} = R/h$ and $\bar{w} = w/b_{\rm id}$, from $\tan\varphi = 2h/b_{\rm id}$ and simple geometrical relations it follows (see Fig. 2) that

$$\bar{w} = \begin{cases} \left(\dfrac{\bar{R}}{\tan(\varphi/2)} - \left[\bar{R}^2 - \left(\bar{x} - \bar{R} \right)^2 \right]^{1/2} \right) \tan\varphi & \text{if } 0 \le \bar{x} \le \bar{R}(1+\cos\varphi), \\ 0 & \text{elsewhere,} \end{cases} \tag{3}$$

where φ is the nominal angle between the lateral sides and bases of prisms in different rows, which is identical to the angle of grazing incidence of the incident beam onto the inclined prism walls. Let us note that the coefficient $\tan\varphi$ is needed for the conversion from the h scale to the $b_{\rm id}$ scale when using unitless variables.

2.2. Focusing of partially coherent radiation by a clessidra lens

In the following we assume a sufficiently monochromatic (wavenumber $2\pi/\lambda$) and a partially coherent incident wavefield on the lens. Thus, the field entering it can be theoretically described by the mutual optical intensity (MOI) function (Williams *et al.*, 2007),

$$J_0(x_1 - x_2) = \psi(x_1)\psi^*(x_2)g(x_1, x_2), \tag{4}$$

where the wavefield spatial coherence length can be specified by the characteristic width of the coherence factor $g(x_1, x_2)$. The above equation is valid for any kind of source, even partially coherent. Only for fully incoherent sources one has $g(x_1, x_2) = g(x_1 - x_2)$ and the MOI formalism becomes equivalent to the simple convolution of the result, obtained for a (coherent) point source, with the Fourier transform of the geometrical source shape. On the other hand, for partially coherent sources this simplification is not possible since it cannot account for the interference of diffraction effects owing to the finite source size with those related to the finite size of the prisms (Shina *et al.*, 1998).

Let us note that for undulator sources the synchrotron radiation emitted by the whole electron beam is determined by the ensemble average in phase space of the two-point product of the X-ray field amplitudes (Wu & Liu, 2005) and, consequently, the X-ray radiation is partially coherent at the source level. Nevertheless, even an undulator can be assimilated to a fully incoherent source of Gaussian shape when the sample-to-source distance is much larger than the source size (Coisson, 1995). Furthermore, assuming that the beam size is sufficiently larger than the coherence length $l_{\rm c}$, the incident waves can be approximated as planar ones with uniform amplitude $\psi(x) = A_0$ and the coherence factor can be written as $g(x_1 - x_2) = \exp[-(x_1 - x_2)^2/2l_{\rm c}^2]$. Thus, from (2) and (4), in terms of unitless variables, the MOI at the lens exit will be given by (Marathay, 1982)

$$J_0(\bar{x}_1 - \bar{x}_2) = \left|A_0\right|^2 \exp\left[-\frac{(\bar{x}_1 - \bar{x}_2)^2}{2\bar{l}_{\rm c}^2} \right] P(j_1, \bar{x}_1)\, P^*(j_2, \bar{x}_2), \tag{5}$$

where the indexes j_1 and j_2 and the corresponding off-axis distances $\bar{x}_1 = x_1/h$ and $\bar{x}_2 = x_2/h$ will, in general, belong to different lens rows; $\bar{l}_{\rm c} = l_{\rm c}/h$.

As we deal with an optical component for synchrotron radiation, we can assume its aperture to be significantly smaller than its distance p from the source. We will also assume it to be small compared with its focal length f. Then we can use the paraxial approximation for the Fresnel propagators, which allows us to calculate the wavefield intensity to any arbitrary distance y from the lens and any off-axis distance $x \ll y$, using the standard paraxial propagation rules (Born & Wolf, 1980; De Caro & Jark, 2008),

$$\begin{aligned} I(\bar{x}, a) = \frac{m_0}{\bar{y}} \Bigg| \sum_{j_1, j_2} \int_{j_2-1/2}^{j_2+1/2} P(j_2, \bar{x}_2) \exp\left[\frac{i\pi m_0}{\bar{y}} (\bar{x}_2 - \bar{x})^2 \right] {\rm d}\bar{x}_2 \\ \times \int_{j_1-1/2}^{j_1+1/2} \exp\left[-\frac{(\bar{x}_1 - \bar{x}_2)^2}{2\bar{l}_{\rm c}^2} \right] P^*(j_1, \bar{x}_1) \\ \times \exp\left[-\frac{i\pi m_0}{\bar{y}} (\bar{x}_1 - \bar{x})^2 \right] {\rm d}\bar{x}_1 \Bigg|. \end{aligned} \tag{6}$$

Here, the unitless variable $\bar{y} = y/(h^2/m_0\lambda)$ has been introduced, which has $\bar{y} = 1$ for $y = f$. The row extremes are individuated by the unitless coordinates $\bar{x}_k = 1/2 + k$, with $k \in \{-N, -N+1, \ldots, -2, -1, 0, 1, 2, \ldots, N-1, N\}$, with $N_{\rm T} = 2N + 1$ being the total number of rows constituting the lens. For normalized

$\bar{l}_c$ values, which are significantly smaller than N_T, the double integral of (6) needs to be solved numerically. This is done for all theoretical predictions, which are compared in the next chapter with experimental data. Instead for $\bar{l}_c \gg N_T$ the coherence factor would be $g = 1$ for all $|\bar{x}_1 - \bar{x}_2|$ and (6) will then refer to the full coherent case. This case was discussed earlier (De Caro & Jark, 2008) with an analytical solution. The present numerical solution gives results which are consistent with it.

3. Experimental data and discussion

3.1. Shape of photon flux distribution in focus

The experiments were performed at BM05 at the ESRF (http://www.esrf.eu/UsersAndScience/Experiments/Imaging/BM05/) with the lens positioned at $q = 53$ m source distance. The experimental data were obtained for a clessidra lens composed of 58 rows of pmma (polymethylmethacrylate, $C_5H_8O_2$, with density 1.19 g cm^{-3}) prisms with straight side walls and with $\varphi = 35^\circ$; $h = 25.67$ µm. For $m_0 = 2$ the latter values result in the optimum operation energy $E = 7.9$ keV, if we use the refractive index from the LBL tabulation $\delta = 4.18 \times 10^{-6}(8.0/E)^2 = 4.29 \times 10^{-6}$ (Henke *et al.*, 1993). We then have $\beta = \delta/435$; $b_{id} = m_0\lambda/\delta = 2\lambda/\delta = 73.2$ µm and $f_{diff} = h^2/m_0\lambda = f_{refr} = h\tan(\varphi)/2\delta = 2.10$ m. A slit with an opening of 1 mm in the focusing direction was put just in front of the lens. The diffracted photon flux was registered by use of a high-resolution X-ray camera with 0.645 µm equivalent pixel size. For the analysis the diffracted photon flux was integrated over 20 µm in the non-focusing direction covering depths in the lens structure between 20 and 40 µm. Data were taken for vertical as well as for horizontal focusing. In both cases the lens was first aligned in angle. Then the optimum photon energy providing minimum photon flux in the secondary peaks was determined, and finally the detector was moved to the position with minimum line width. The independent alignment in both orientations resulted in identical optimum position within the operated increments of 0.1 keV and 0.01 m. In fact, minimum photon flux in the secondary maxima was found for a photon energy of 7.9 keV, consistent with the expectation for the present lens structure. The minimum line width was found for $y = 2.16 \pm 0.01$ m which is compatible with the expected image position. In Fig. 3 we compare these experimental data (open circles) with the results obtained from our model (continuous curves). The agreement is very good, especially if we consider that it has been obtained assuming the projected values in the theoretical model for all parameters, except for the finite spatial coherence and the presence of finite spherical menisci. The calculations then use $m_0 = 2$, $\Delta m = 0$, $\bar{y} = 1$ and $s = 0$. Note that we have assumed a planar incident wavefield and thus we cannot take into account corrections of the focus position owing to the finite distance between the source and lens. Theoretically the best image is thus to be found in the focal plane for $\bar{y} = 1$. From the simulations we find $\bar{l}_{c,ver} = 0.95 \pm 0.05$ and $\bar{l}_{c,hor} = 0.55 \pm 0.05$ for the vertically and horizontally focusing configuration, respectively. These results correspond to coherence lengths of about 24.0 ± 1.5 µm and 14.0 ± 1.5 µm, respectively.

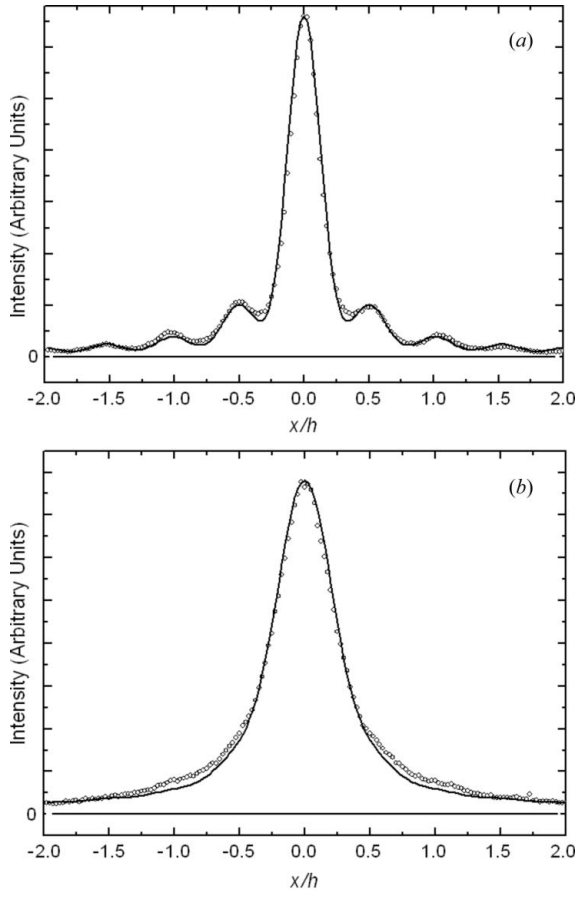

Figure 3
(*a*) Open circles represent the measured intensity distribution in the best image plane for the vertical configuration. The line is the related simulation for (see main text for symbol explanation) $m_0 = 2.0$; $\Delta m = 0$; $\bar{y} = 1.0$; $R = 2.8$ µm; $\bar{w} = 0$; $\bar{s} = 0$ and $\bar{l}_c = 0.95$. The intensities are given in arbitrary units and are made to coincide in the maximum. (*b*) Same as in (*a*) but for the horizontal configuration. The simulation (line) is for the same parameters except $\bar{l}_c = 0.55$.

During our experiments with exposure times of $t > 200$ s the vertical source size appeared to be virtually doubled compared with the electron beam size to about $S = 170$ µm. This was due to unidentified aperiodic vibrations in the beam transport system with frequencies in the hertz range (Jark *et al.*, 2008). In the horizontal direction the source size was $S = 269$ µm. Then, according to Attwood (1999), $l_c = 0.44\lambda q/S$, and the estimated lateral coherence lengths of the incident beam at the lens position orthogonal to the optical axis are about 21.5 µm in the vertical direction and 13.6 µm in the horizontal direction. Considering the uncertainty, especially in the vertical source size, the simulations and the experiments are in rather good agreement. As far as the measured peak width is concerned, it has to be noted that significantly smaller FWHM values were found in earlier experiments, when we used larger spatial coherence lengths for lenses with identical focal length (Jark *et al.*, 2004). For the radius of the menisci we find $R = 2.8 \pm 0.2$ µm, which is a reasonable number, compatible with measurements made with an optical microscope on the lens surface.

Although some small differences between simulated and measured intensities are evident in Fig. 3, the good agreement with the experimental data obtained by using only two free parameters is an important validation of the theoretical model. Our simulations indicate that (i) the coherence length mostly affects the width of the peaks; (ii) the intensity in the first secondary peaks is mostly due to the field distortion in the straight prism side walls; (iii) the presence of the menisci mostly affects the intensity in higher-order peaks and in interpeak positions.

3.2. Focusing performances of a clessidra lens

According to Liouville's theorem the density in phase space, *i.e.* the number of photons per unit of time, energy, solid angle and area, is constant along a photon beam in a vacuum (Arndt, 1990). For any collimating system, whether focusing or not, this theorem gives us the possibility to define the enhancement E_i of the angular divergence owing to the lens as follows,

$$E_i = \mathrm{NA}_{\mathrm{lens}} / \mathrm{NA}_{\mathrm{source}}. \quad (7)$$

NA denotes the numerical aperture which, in respect to a given point P, depends on the half-angle of the maximum cone of radiation that can enter or exit an optical object, as seen by P. In fact, the action of the lens can be described as a change in phase space of the beam angular width. According to Liouville's theorem, this finding causes a change of the maximum intensity, leading to a focusing behaviour. Since the real source profile used in the experiment is actually unknown, we put $\mathrm{NA}_{\mathrm{source}} \simeq S_i/q$, where S_i is the vertical (horizontal) FWHM of the source. Furthermore, for the NA of the lens, we can put $\mathrm{NA}_{\mathrm{lens}} \simeq A_{\mathrm{eff}}/2f$. The effective aperture A_{eff} is the lens transmission function $t(x)$ integrated over the lens aperture and it is given for a clessidra by Jark *et al.* (2004). We can also define an effective number of lens rows $N_{\mathrm{T,eff}} = A_{\mathrm{eff}}/h = \bar{A}_{\mathrm{eff}}$, which is a unitless parameter expressing the effective aperture. Thus, from (7) and the definition of the lens diffractive focus distance [equation (1)], we find for E_i,

$$E_i = \frac{m l_{c,i} N_{\mathrm{T,eff}}}{0.88h} = \frac{l_{c,i}}{d_{\mathrm{coh}}}, \quad (8)$$

where d_{coh} is the minimum lens focus size obtainable for full coherent incident radiation (De Caro & Jark, 2008). This quantity will be related to either the effective aperture of the lens or to the size of any slit put just before the lens. When $l_{c,i} > N_{\mathrm{T,eff}}h$, we deal once more with a full coherent incident beam. In this case the lens focusing efficiency according to (8) is limited by the effective number of rows constituting the lens, and it is thus better written as $E_i = \min(N_{\mathrm{T,eff}}, \bar{l}_{c,i})/\bar{d}_{\mathrm{coh}}$. The usefulness of the quantity defined in (8) is related to the possibility to directly evaluate the effects of the lens defects and of the finite coherence on the lens focusing performance.

The experimental results described in the previous section refer to a 1 mm slit in front of the lens. In this case, with R = 2.8 µm, $m_0 = 2$, one has $N_{\mathrm{T,eff}} \simeq 0.73 \times 39 \simeq 28.5$ (Jark *et al.*, 2004). This leads to $d_{\mathrm{coh}} = 0.0154h$ and $E_i \simeq 64.8\bar{l}_{c,i}$. For full coherent incident radiation and perfect lenses one would have an upper limit of $\bar{l}_{c,i} = N_{\mathrm{T,eff}}$ and, therefore, a maximum value for the angular-divergence enhancement given by $E_{\mathrm{coh}}(1\ \mathrm{mm}) = 1846$. The experimental data instead lead to only partially coherent illumination in the 1 mm aperture with $\bar{l}_{c,\mathrm{ver}} = 0.95 \pm 0.05$ in the vertical direction and $\bar{l}_{c,\mathrm{hor}} = 0.55 \pm 0.05$ in the horizontal, for which we would thus expect ideally $E_{\mathrm{v,theo}} \simeq 62 \pm 3$ and $E_{\mathrm{h,theo}} \simeq 36 \pm 3$. On the other hand, the measured values are found to be smaller with $E_{\mathrm{v,exp}} \simeq 39 \pm 1$ and $E_{\mathrm{h,exp}} \simeq 23 \pm 1$. As would have to be expected, the ratios $E_{\mathrm{v,exp}}/E_{\mathrm{v,theo}} = 0.63 \pm 0.04$ and $E_{\mathrm{h,exp}}/E_{\mathrm{h,theo}} = 0.64 \pm 0.06$ are identical within their errors, and they should be caused by the lens defects, such as the spherical menisci and the deviation from the perfect parabolic lens profile, which diffract the transmitted radiation away from the main maximum.

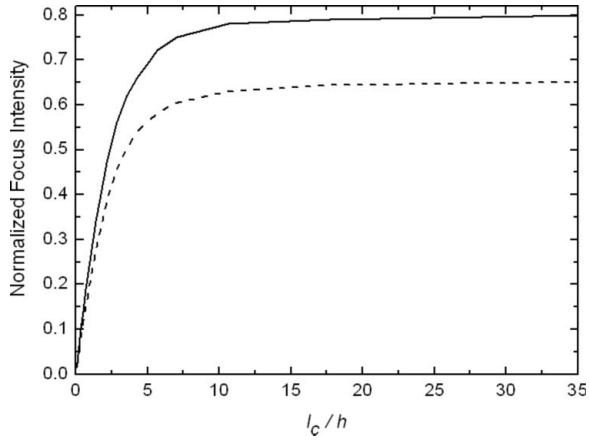

Figure 4
Maximum intensity in the focus ($\bar{x} = 0, \bar{y} = 1$), normalized with respect to $m_0 N_{\mathrm{T}}^2$, as a function of $\bar{l}_c$. The calculations are for the material and lens properties used in Fig. 3 and for $N_{\mathrm{T}} = 7$. The continuous and the dashed curves have been obtained for $R = 0$ and $R = 2.8$ µm, respectively.

In Fig. 4 we show the maximum intensity in the center of the diffraction pattern ($\bar{x} = 0, \bar{y} = 1$) obtained from (6), normalized with respect to $m_0 N_{\mathrm{T}}^2$, as a function of $\bar{l}_c$. All parameters are identical to those used for the simulations in Fig. 3. We have considered $m_0 = 2$. The continuous and dashed curves have been obtained for $R = 0$ µm and for $R = 2.8$ µm, respectively. We can note that for $R = 0$ (continuous curve) the normalized maximum reaches about 0.80 of the value predicted by the full coherent theoretical model (De Caro & Jark, 2008) for the ideal parabolic lens. This reduction is caused by the deviation of the clessidra profile with straight prisms from the parabolic profile. For $R = 2.8$ µm (dashed curve) the normalized maximum is further reduced by another factor of about 0.8 to 0.65. This latter value is now in agreement with the measured ratios $E_{\mathrm{v,exp}}/E_{\mathrm{v,theo}}$ and $E_{\mathrm{h,exp}}/E_{\mathrm{h,theo}}$ within the experimental errors.

4. Conclusions

We have presented a numerical theoretical attempt for the prediction of the diffracted intensity in the image plane of a clessidra lens, when the latter is only partly coherently illuminated. Currently experimental data for kinoform (Fresnel) X-ray lenses are mostly taken in this condition. Related

experimental data are thus confronted with the calculations with this numerical model. In the experiment the spatial coherence length could be varied. The simulations show that the presented experimental data are consistent with operation of the lens in the optimum conditions for photon energy and detector position. Also the refractive index for the lens material pmma from tabulations is applicable to our samples and the projected lens parameters $\varphi = 35^\circ$ and $h = 25.67$ μm are confirmed. Only two more free parameters were needed in order to simulate well the experimental intensity distributions. The first is the spatial coherence length, which is directly correlated with the image size. This parameter is found in very good agreement with the expectations for the two orthogonal source sizes. The second parameter is a rounding of the tips and edges of the prisms during the production. In this case a radius of curvature of $R = 2.8$ μm for a spherical meniscus needs to be assumed. These numbers lead not only to the best qualitative agreement between the measured and the calculated intensity distribution but also to the best quantitative description of the focusing performances of clessidra lens. Then if we would like to stay with the straight prism concept, the only loss mechanism assignable to a lens defect is the presence of the rounding of all tips and shallow corners in the prism structure. The present result of $R = 2.8$ μm will make clessidra lenses with the earlier discussed $h = 4$ μm for $f = 0.1$ m unfeasible. However, if we can improve our production technique to state-of-the-art in lithography with values of the order of $R = 1$ μm (Nazmov *et al.*, 2004), the same data set will be feasible with acceptable losses. It should be noted that the aperture of such lenses will still be difficult to fill with completely spatially coherent radiation. When this is possible the focus size will be very competitive with those which can be obtained with other focusing devices. However, until X-ray sources of new generation are available, focusing by use of a clessidra will continue to be source size limited and the data interpretation will still require the presented treatment for partially coherent illuminations.

We gratefully acknowledge the help provided during the experiment by I. Snigireva and A. Snigirev from ESRF.

References

Aristov, V., Grigoriev, M., Kuznetsov, S., Shabelnikov, L., Yunkin, V., Weitkamp, T., Rau, C., Snigireva, I., Snigirev, A., Hoffmann, M. & Voges, E. (2000). *Appl. Phys. Lett.* **77**, 4058–4060.

Arndt, U. W. (1990). *J. Appl. Cryst.* **23**, 161–168.

Attwood, D. (1999). *Soft X-rays and Extreme Ultraviolet Radiation: Principles and Applications*, ch. 8. Cambridge University Press.

Born, M. & Wolf, E. (1980). *Principle of Optics*, 6th ed. New York: Pergamon.

Cederström, B., Ribbing, C. & Lundqvist, M. (2005). *J. Synchrotron Rad.* **12**, 340–344.

Coisson, R. (1995). *Appl Opt.* **34**, 904–906.

De Caro, L. & Jark, W. (2008). *J. Synchrotron Rad.* **15**, 176–184.

Evans-Lutterodt, K., Ablett, J. M., Stein, A., Kao, C.-C., Tennant, D. M., Klemens, F., Taylor, A., Jacobsen, C., Gammel, P. L., Huggins, H., Ustin, S., Bogart, G. & Ocola, L. (2003). *Opt. Express*, **11**, 919–926.

Evans-Lutterodt, K., Stein, A., Ablett, J. M., Bozovic, N., Taylor, A. & Tennant, D. M. (2007). *Phys. Rev. Lett.* **99**, 134801.

Henke, B. L., Gullickson, E. M. & Davis, J. C. (1993). *Atom. Data Nucl. Data Tables*, **54**, 181–342 (http://www-cxro.lbl.gov/optical_constants/).

Jark, W., Matteucci, M. & Menk, R. H. (2008). *J. Synchrotron Rad.* **15**, 411–413.

Jark, W., Pérennès, F. & Matteucci, M. (2006). *J. Synchrotron Rad.* **13**, 239–252.

Jark, W., Pérennès, F., Matteucci, M., Mancini, L., Montanari, F., Rigon, L., Tromba, G., Somogyi, A., Tucoulou, R. & Bohic, S. (2004). *J. Synchrotron Rad.* **11**, 248–253.

Kohn, V., Snigireva, I. & Snigirev, A. (2003). *Opt. Commun.* **216**, 247–260.

Lengeler, B., Schroer, C., Tümmler, J., Benner, B., Richwin, M., Snigirev, A., Snigireva, I. & Drakopoulos, M. (1999). *J. Synchrotron Rad.* **6**, 1153–1167.

Lesem, L. B., Hirsch, P. M. & Jordan, J. A. Jr (1969). *IBM J. Res. Dev.* **13**, 150–155.

Marathay, A. S. (1982). *Elements of Optical Coherence Theory*, pp. 182–185. New York: Wiley.

Nazmov, V., Shabel'nikov, L., Pantenburg, F.-J., Mohr, J., Reznikova, E., Snigirev, A., Snigireva, I., Kouznetsov, S. & DiMichiel, M. (2004). *Nucl. Instrum. Methods Phys. Res. B*, **217**, 409–416.

Nöhammer, B., Hoszowska, J., Freund, A. K. & David, C. (2003). *J. Synchrotron Rad.* **10**, 168–171.

Pérennès, F., Matteucci, M., Jark, W. & Marmiroli, B. (2005). *Microelectron. Eng.* **78–79**, 79–87.

Schroer, C. G., Kurapova, O., Patommel, J., Boye, P., Feldkamp, J., Lengeler, B., Burghammer, M., Riekel, C., Vincze, L., van der Hart, A. & Küchler, M. (2005). *Appl. Phys. Lett.* **87**, 124103.

Shina, S. K., Tolan, M. & Gibaud, A. (1998). *Phys. Rev. B*, **57**, 2740–2758.

Snigirev, A., Kohn, V., Snigireva, I. & Lengeler, B. (1996). *Nature (London)*, **384**, 49–51.

Snigirev, A., Kohn, V., Snigireva, I., Souvorov, A. & Lengeler, B. (1998). *Appl. Opt.* **37**, 653–660.

Suehiro, S., Miyaji, H. & Hayashi, H. (1991). *Nature (London)*, **352**, 385–386.

Williams, G. J., Quiney, H. M., Peele, A. G. & Nugent, K. A. (2007). *Phys. Rev. B*, **75**, 104102–104109.

Wu, X. & Liu, H. (2005). *Appl. Opt.* **44**, 5847–5854.